Valence Control of Ionic Molecular Crystals: Effect of Substituents on the Structures and Valence States of Biferrocenium Salts with Fluoro Tetracyanoquinodimethanides

Mochida, Tomoyuki ; Funasako, Yusuke ; Kimata, Hironori ; Tominaga, Takumi ; Sakura, Takahiro ; Ohta, Hitoshi

(Citation)
Crystal Growth & Design,17(11):6020-6029

(Issue Date)
2017-11

(Resource Type)
journal article

(Version)
Accepted Manuscript

Valence Control of Ionic Molecular Crystals: Effect of Substituents on the Structures and Valence States of Biferrocenium Salts with Fluoro tetracyanoquinodimethanides

Tomoyuki Mochida,[*,†] *Yusuke Funasako,*[‡] *Hironori Kimata,*[†] *Takumi Tominaga,*[†] *Takahiro Sakurai,*[§] *and Hitoshi Ohta*[¶,#]

[†]Department of Chemistry, Graduate School of Science, Kobe University, Kobe, Hyogo 657-8501, Japan

[‡]Department of Applied Chemistry, Faculty of Engineering, Tokyo University of Science, Yamaguchi, Sanyo-Onoda, Yamaguchi 756-0884, Japan

[§]Research Facility Center for Science and Technology, Kobe University, Kobe, Hyogo 657-8501, Japan

[¶]Department of Physics, Graduate School of Science, Kobe University, Kobe, Hyogo 657-8501, Japan

[#]Molecular Photoscience Research Center, Kobe University, Kobe, Hyogo 657-8501, Japan

ABSTRACT: In this work, the effect of substituents on the valence states of biferrocenium salts was investigated in order to explore the valence control of ionic molecular materials. Reactions of 1′,1‴-disubstituted biferrocene derivatives (R_2-bifc) and fluoro tetracyanoquinodimethanes (F_n-TCNQ; n = 1, 2, 4) produced single crystals of six salts (**1**–**6**), most of which were either monovalent ($[D]^+[A_m]^-$; m = 1–3) or divalent ($[D]^+[A_m]^-$) salts. (Et_2-bifc)(F_1-TCNQ)$_2$ (**1**) was a

mixed-stack monovalent salt, whereas the corresponding F_2-TCNQ salt was a divalent salt. (MeO_2-bifc)(F_1-TCNQ)$_2$ (**2**) was a monovalent salt because of the small Madelung energy of its segregated-stack structure, despite the low redox potential of the donor. (MeS_2-bifc)(2,6-F_2-TCNQ)$_2$ (**3**) was a mixed-stack salt with an apparent intermediate valence state ($[D]^{1.5+}[A_2]^{1.5-}$), containing $[D]^{2+}$ and $[D]^{+}$ in a 1:1 ratio. Its valence state, which is intermediate between those of corresponding salts with F_1-TCNQ and 2,5-F_2-TCNQ, is probably related to the unsymmetrical crystalline environment. (Bu_2-bifc)(F_1-TCNQ)$_3$ (**4**) was a divalent salt with a segregated-stack structure, whereas the corresponding TCNQ salt was monovalent. (R_2-bifc)(F_4-TCNQ) [R = Bu (**5**), I (**6**)] were monovalent salts. Their magnetic susceptibilities were found to be consistent with their valence states. These results demonstrated that the valence control of biferrocenium salts could be achieved via the fluorine substitution of acceptors and crystal engineering.

INTRODUCTION

Controlling the valence states of solids is an important aspect of solid-state electronics. To date, many studies have been conducted on charge-transfer salts consisting of donor (D) and acceptor (A) units. These studies have attracted significant attention from the viewpoint of their unique electronic properties and phase transition phenomena.[1,2] The modification of the valence states of these materials leads to variations in their physical properties. Electron-transfer salts containing biferrocenium cations have been investigated mainly because of their interesting valence states.[3–9] Stepwise oxidation of biferrocene produces a monocation ($[D]^{+}$) containing Fe^{II} and Fe^{III} and a dication ($[D]^{2+}$) containing two Fe^{III} (Figure 1a) centers. The monocation exhibits either a valence-detrapped state based on valence tautomerization (Figure 1b) or a valence-trapped state. Furthermore, the valence state may depend on the temperature. The

valence state is largely influenced by molecular symmetry and the crystalline environment. Hence, biferrocenium salts are useful for investigating correlations between valence states and intermolecular interactions in molecular crystals.

We have previously investigated the crystal structures and valence states of biferrocenium salts with tetracyanoquinodimethane (TCNQ) and other organic acceptors, and found that these salts exhibit intriguing electronic properties and phase transition phenomena.[10–12] These salts generally exist in 1:1–1:3 D/A ratios and their crystal structures can be classified into mixed-stack structures with alternating donor/acceptor stacking, segregated-stack structures with independent columnar π–π stacking of donors and acceptors, or an intermediate type (Figure 2a).[12,14,15] However, unlike organic charge-transfer complexes, there are often π–π contacts between the acceptors (or acceptor dimers) even in mixed-stack structures because of the nonplanar shape of the donor. Biferrocenium–TCNQ salts exhibit either monovalent state ($[D]^{+}[A_m]^{-}$; m = 1–3) or divalent state ($[D]^{2+}[A_m]^{2-}$) (Figure 2b), depending on the balance between the redox potentials of the constituent molecules and the Coulombic (Madelung) energies of the crystal.[12–15] The Madelung energies depend on the charges, volumes, and arrangements of the constituent molecules. There are also a few biferrocenium–TCNQ salts that contain both $[D]^{+}$ and $[D]^{2+}$.[14,16] A phase boundary between the monovalent and divalent salts has been determined for the mixed-stack 1:2 D/A structures (Figure 3).[13] This figure shows the correlation of the valence states with ΔE (difference of the redox potentials of $D^{+/2+}$ and $A_2^{-/2-}$) and the unit cell volume. Furthermore, a phase transition was observed between the monovalent and divalent states of (neopentyl$_2$-bifc)(F$_1$-TCNQ)$_3$.[10] This valence-transformation phenomenon is related to the neutral–ionic transition in organic charge-transfer complexes.[2]

In this study, to further investigate the effect of substituents on the structures and valence

states of biferrocenium–TCNQ salts, 1′,1‴-R_2-1,1″-biferrocene (R_2-bifc) with various substituents (R = Et, MeO, MeS, Bu, I, and CN) was reacted with F_n-TCNQ (n = 1, 2, 4; Figure 4). The donor substituents were chosen for their varying electron donating abilities; MeO_2-bifc and CN_2-bifc are the strongest and weakest electron donors, respectively, to have ever been used for complexation with TCNQ derivatives. The electron accepting ability of F_n-TCNQs increases with increasing number of fluorine atoms. 2,6-F_2-TCNQ is a polar isomer of 2,5-F_2-TCNQ (= F_2-TCNQ) that is used to investigate the effect of acceptor polarity.[17] As a result, six salts with D/A ratios in the range of 1:1–1:3, (R_2-bifc)(F_1-TCNQ)$_2$ [R = Et (**1**), R = MeO (**2**)], (MeS_2-bifc)(2,6-F_2-TCNQ)$_2$ (**3**), (Bu_2-bifc)(F_1-TCNQ)$_3$ (**4**), and (R_2-bifc)(F_4-TCNQ) [R = ^{n}Bu (**5**), R = I (**6**)] were obtained and characterized. Structurally, they are closely related to the previously reported salts with other substituents, enabling a clear discussion of the effect of substituents and crystal structures on their properties. In particular, a remarkable effect of the fluorine substitution of the acceptor on the valence states of these salts was observed. The redox potential and crystal structure of CN_2-bifc have also been reported.

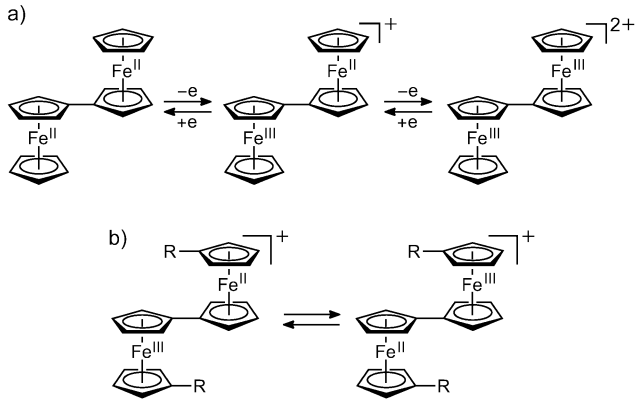

Figure 1. (a) Three redox states of biferrocene. (b) Valence tautomerization of the mixed-valence 1′,1‴-R_2-1,1″-biferrocenium cation. Molecules with R = Et, MeO, MeS, Bu, I, and CN were used in this study.

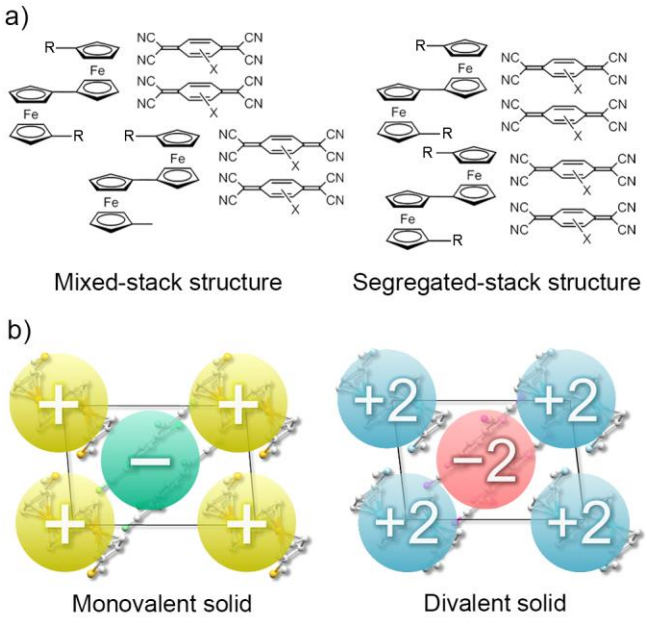

Figure 2. (a) Schematic illustrations of the assembled structures of biferrocenium–TCNQ salts: mixed-stack (left) and segregated-stack (right) structures. The case of 1:2 D/A salts is shown. (b) Schematic illustrations of monovalent (left) and divalent (right) 1:2 D/A biferrocenium salts with mixed-stack structures.

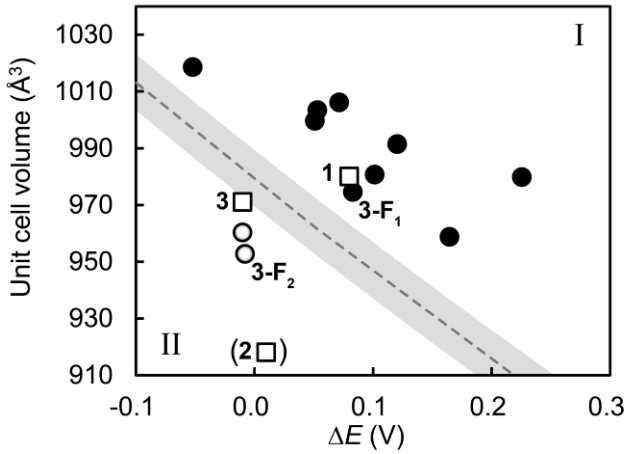

Figure 3. Monovalent-divalent phase diagram[13] showing the correlation of valence states with ΔE (difference of the redox potentials of D^+ and A_2^-) and unit cell volume (at 173 K) for mixed-stack 1:2 D/A biferrocenium–TCNQ salts. The dotted line is the boundary between the monovalent (●) and divalent (○) salts, and the gray area is a two-phase coexistence region. The

diagram includes the salts obtained in the current study (□; **1**−**3**), of which the plot for **2** is tentative (shown in parenthesis) because it has a segregated-stack structure (see text).

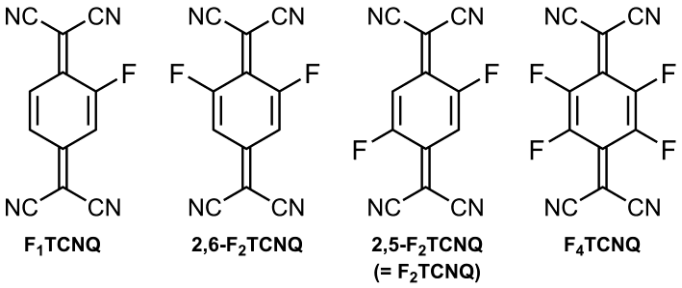

Figure 4. Structural formulae of F$_n$-TCNQ used in the current study.

RESULTS AND DISCUSSION

Valence states. The stoichiometry and valence states of **1**–**6**, determined based on X-ray structures, are summarized in Table 1. Salt **6** was a dichloromethane solvate, which is the sole example of a solvate crystal for biferrocenium–TCNQ salts. The donor–acceptor ratios and valence states (I: monovalent, II: divalent) of **1**–**6** and related salts[12,13,15] are summarized in Table 2. Half of the salts are newly synthesized in the current study. It is evident that a majority of these salts have a 1:2 D/A ratio, whereas the F_4-TCNQ salts have a 1:1 ratio and the Bu_2-bifc salts with F_1-TCNQ or TCNQ have a 1:3 ratio. In the 1:2 salts, F_1-TCNQ produces monovalent salts. In contrast, F_2-TCNQ tends to produce divalent salts, demonstrating the effect of fluorine substitution on the valence states.

The valence states of cations in **1**–**6** are discussed first, based on their molecular structures. The ORTEP drawings of the cations are shown in Figure 5. The cations in **1**, **2**, and **4** are located on inversion centers, exhibiting centrosymmetric structures. The substituents in **2** and **5** exhibited a two-fold disorder (0.5:0.5). The valence state of the biferrocene derivatives can be estimated

from the Fe–$Cp_{centroid}$ distance (Cp = cyclopentadienyl ring); the distances are approximately 1.655 Å and 1.705 Å for neutral (Fc^0) and cationic (Fc^+) ferrocenyl moieties, respectively, and a valence-detrapped monocation ($Fc^{+0.5}$–$Fc^{+0.5}$) has an average distance of 1.68 Å.[14] The Fe–Cp distances in **1**–**6** are summarized in Figure 6 and Table 3. The values indicate that **1** and **2** (Fe–Cp = 1.68 Å) contain valence-detrapped biferrocenium monocations ($Fc^{+0.5}$–$Fc^{+0.5}$). The cation in **3** has an unusual intermediate cation valence state (Fc^+–$Fc^{+0.5}$), in which the Fe1-containing moiety is cationic (Fe–Cp = 1.705 Å) and the other moiety is intermediate between neutral and cationic (Fe–Cp = 1.684 Å). The Fe–Cp distances in **3** were temperature-independent (293–100 K), indicating that no changes occurred in the valence state. Therefore, the structure of salt **3** was interpreted as having $[D]^+$ and $[D]^{2+}$ exist in a 1:1 ratio to produce an averaged $[D]^{+1.5}$ structure. A similar valence state has been found in (^{i}PrS$_2$-bifc)$_2$(F_4-TCNQ)$_3$.[14] Salt **4** (Fe–Cp = 1.71 Å) contains a biferrocenium dication (Fc^+–Fc^+), whereas **5** and **6** contain valence-trapped monocations (Fc^+–Fc^0), in which the Fe1-containing moiety is cationic.

The charges on the acceptors were estimated from the intramolecular bond lengths[13,14] using the Kistenmacher relation.[18] These values are listed in Table 1, which are consistent with the cation charges. The acceptor charges in **1** and **2** ($[D]^+[A_2]^-$) were approximately −0.5, and the charge in **3** ($[D]^{1.5+}[A_2]^{1.5-}$) was approximately −1.5 per dimer (= −0.67−0.80). However, the estimated charge for **4** ($[A_3]^{-1.4}$, where –1.4 = −0.57×2−0.27) deviated from the supposed valence state ($[D]^{2+}[A_3]^{2-}$), probably because of the effects of disorder. The charges in **5** and **6** ($[D]^+[A]^-$) were approximately −1. The acceptors formed dimeric arrangements in the salts, with the exception of **4**. The intermolecular distances in the dimer were longer for $[A_2]^-$ (3.99 Å in **1** and 3.46 Å in **2**) than for $[A_2]^{2-}$ (3.21 Å in **5** and 3.26 Å in **6**, centroid–centroid distance). This shorter distance in the latter occurs because of the formation of diamagnetic dimers.[13] The corresponding distance in the intermediate-valence salt **3** (3.30 Å) falls between those of $[A_2]^-$ and $[A_2]^{2-}$.

The structurally determined valence states are further supported by magnetic measurements, as shown in the next section. Details of the crystal structure and valence state for each salt are discussed in the section on crystal structures.

Table 1. Summary of valence states and structures of **1**–**6**.

D/A ratio	salts	valence state	valence state of monocation	structure type	acceptor charge[a]
1:2 salts	(Et_2-bifc)(F_1-TCNQ)$_2$ (**1**)	$[D]^+[A_2]^-$	detrapped	1:2 mixed-stack	−0.47
	(MeO_2-bifc)(F_1-TCNQ)$_2$ (**2**)	$[D]^+[A_2]^-$	detrapped	segregated-stack	−0.58
	(MeS_2-bifc)(2,6-F_2-TCNQ)$_2$ (**3**)	$[D]^{1.5+}[A_2]^{1.5-}$ [b]	trapped	1:2 mixed-stack	−0.67[c,e], −0.80[d,e]
1:3 salt	(Bu_2-bifc)(F_1-TCNQ)$_3$ (**4**)	$[D]^{2+}[A_3]^{2-}$	–	segregated-stack	−0.57[c], −0.27[d]
1:1 salts	(Bu_2-bifc)(F_4-TCNQ) (**5**)	$[D]^+[A]^-$	trapped	2:2 mixed-stack	−0.97
	(I_2-bifc)(F_4-TCNQ)·0.5CH_2Cl_2 (**6**)	$[D]^+[A]^-$	trapped	(solvate crystal)	−0.91

[a]Estimated based on the structures of F_1TCNQ$^{0/-1}$ and F_4-TCNQ$^{0/-1}$ using the Kistenmacher relation.[18] Averaged structures of TCNQ$^{0/-1}$ and F_4TCNQ$^{0/-1}$ were used for 2,6-F_2-TCNQ. The bond lengths of the three bonds opposite the F atom were used for F_1-TCNQ. [b]Averaged structure of monovalent and divalent states, in which the monocation exhibits the valence-trapped state (see text). [c]Charge on molecule A1. [d]Charge on molecule A2. [e]Based on the structure at 293 K.

Table 2. Donor–acceptor ratios (1:*n*) in **1**–**6** and related salts. Valence states are shown in square parentheses (I: monovalent, II: divalent).

Salts	Donor (D)				
	Bu_2-bifc	Et_2-bifc	MeO_2-bifc	MeS_2-bifc	I_2-bifc
(D)(TCNQ)$_n$	1:3 [I][a]				
(D)(F_1-TCNQ)$_n$	1:3 [II] (**4**)	1:2 [I] (**1**)	1:2 [I] (**2**)	1:2 [I][b]	
(D)(2,6-F_2-TCNQ)$_n$				1:2 [I-II][d] (**3**)	
(D)(F_2-TCNQ)$_n$		1:2 [II][b]		1:2 [II][b]	1:2 [I][c]
(D)(F_4-TCNQ)$_n$	1:1 [I] (**5**)	1:1 [I][a]			1:1[I] (**6**)

[a]Ref. 12. [b]Ref. 13, [c]Ref. 15. [d]1:1 mixture of monocation and dication (see text).

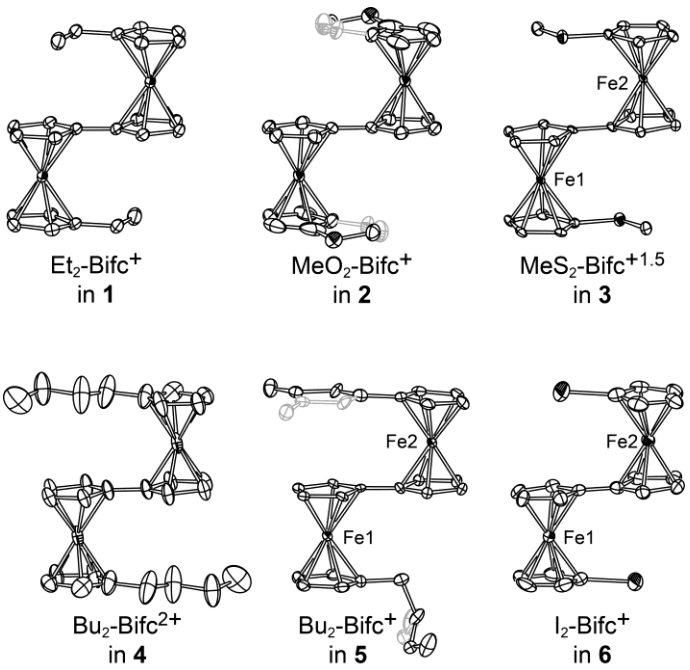

Figure 5. ORTEP drawings of the cations in **1**–**6**. One of the disordered moieties in **2** and **5** is displayed in gray. Hydrogen atoms have been omitted for clarity.

Table 3. Interatomic distances around the Fe atom in the cations in **1**–**6** and in CN_2-bifc.

compounds	Fe site	Fe–Cp[a] / Å	Fe–C(Cp)[b] / Å
1		1.682	2.071 [2.113(3)–2.051(3)]
2		1.683	2.062 [2.10(1)–2.029(6)]
3 (100 K)	Fe1	1.705	2.094 [2.151(3)–2.061(2)]
	Fe2	1.684	2.077 [2.122(3)–2.049(3)]
3 (200 K)	Fe1	1.704	2.090 [2.146(2)–2.060(2)]
	Fe2	1.683	2.073 [2.119(2)–2.046(2)]
3 (293 K)	Fe1	1.705	2.088 [2.143(3)–2.056(3)]
	Fe2	1.681	2.070 [2.117(3)–2.042(3)]
4		1.707	2.091 [2.121(7)–2.071(8)]
5	Fe1	1.696	2.083 [2.135(8)–2.047(7)]
	Fe2	1.651	2.050 [2.073(11)–2.040(8)]
6	Fe1	1.707	2.090 [2.141(8)–2.063(9)]
	Fe2	1.657	2.048 [2.07(1)–2.030(9)]
CN_2-bifc		1.654	2.049 [2.072(3)–2.029(4)]

[a]Distance between Fe and centroid of Cp ring (average value).

[b]Average value. Distance range is shown in parenthesis.

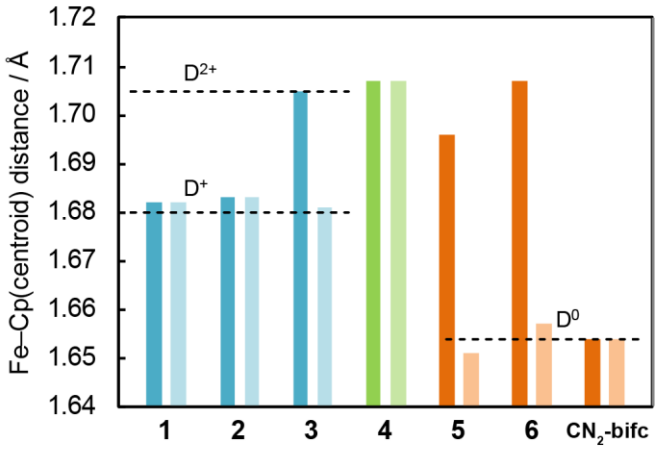

Figure 6. Average Fe–$Cp_{centroid}$ distances in the cations in **1**–**6**. The distance in the case of CN_2-bifc is also shown. The distances for ferrocenyl moieties containing Fe1 (left) and Fe2 (right) are shown for each salt, whereas those in **1**, **2**, **4**, and CN_2-bifc are symmetry related. The average distances for D^{2+}, D^+ (valence-detrapped monocation), and D^0 are indicated by dotted lines.

Magnetic susceptibilities. We measured the temperature dependence of the magnetic susceptibilities of **2**–**4** and **6** in order to verify their valence states. It was found that the salts did not show any valence transitions in the temperature range of 2–300 K.

The magnetic susceptibilities of (MeO_2-bifc)(F_1-TCNQ)$_2$ (**2**), (Bu_2-bifc)(F_1-TCNQ)$_3$ (**4**), and (I_2-bifc)(F_4-TCNQ)·0.5CH_2Cl_2 (**6**) are shown as the χT vs. T plot in Figure 7a. The room temperature χT values for these salts were 0.75, 1.2, and 0.6 emu K mol^{-1}, respectively. As one ferrocenium spin accounts for 0.6 emu K mol^{-1},[14] these values support our assessment that **2** and **6** are monovalent salts containing $[D]^+$, and that **4** is a divalent salt containing $[D]^{2+}$. The contributions of the acceptor spins are probably suppressed by the intermolecular antiferromagnetic interactions.

The magnetic susceptibility of **3** is plotted in Figure 7b, together with the susceptibilities of

the corresponding F_1-TCNQ ((MeS$_2$-bifc)(F_1-TCNQ), **3-F$_1$**) and F_2-TCNQ ((MeS$_2$-bifc)(F_2-TCNQ), **3-F$_2$**) salts. **3-F$_1$** and **3-F$_2$** were monovalent ($[D]^+[A_2]^-$) and divalent ($[D]^{2+}[A_2]^{2-}$) salts, respectively.[13] The magnetic susceptibility of **3** was intermediate between the values of **3-F$_1$** and **3-F$_2$** in the entire measured temperature range, which is consistent with the presence of $[D]^{2+}$ and $[D]^+$ in a 1:1 ratio. The decrease in the magnetic moment with decreasing temperature in the case of **3-F$_2$** is typical of sulfur-containing biferrocenium dications, which originates from the loss of orbital contributions and intramolecular antiferromagnetic interactions.[16a]

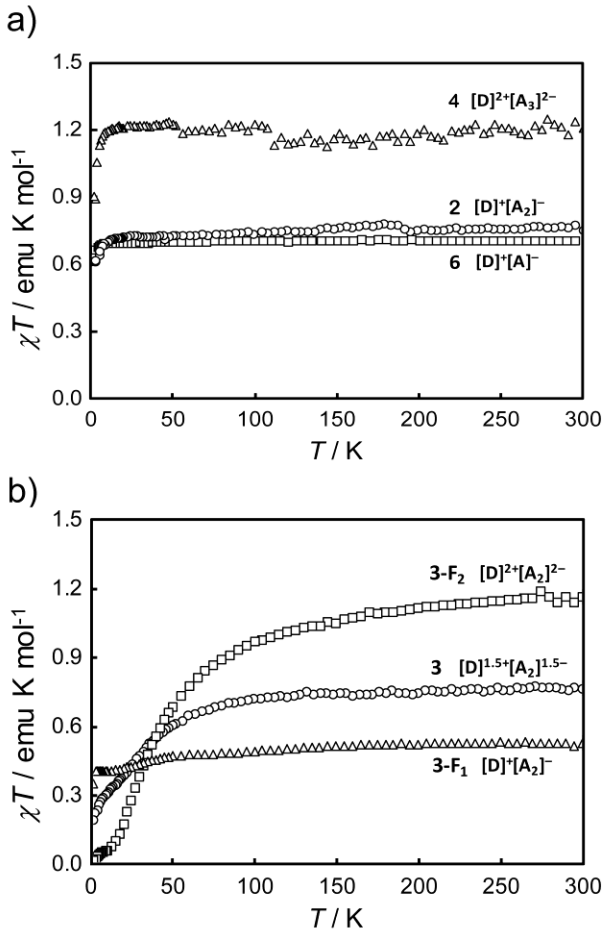

Figure 7. Temperature dependence of the magnetic susceptibilities represented as the χT vs. T plot. (a) (MeO$_2$-bifc)(F_1-TCNQ)$_2$ (**2**), (Bu$_2$-bifc)(F_1-TCNQ)$_3$ (**4**), and

(I_2-bifc)(F_4-TCNQ)·0.5CH_2Cl_2 (**6**). (b) (MeS_2-bifc)(2,6-F_2-TCNQ)$_2$ (**3**), (MeS_2-bifc)(F_1-TCNQ)$_2$ (**3-F$_1$**), and (MeS_2-bifc)(F_2-TCNQ)$_2$ (**3-F$_2$**). The data for **3-F$_1$** and **3-F$_2$** are taken from Ref. 13.

Structures of monovalent F$_1$-TCNQ salts (1 and 2). (Et_2-bifc)(F_1-TCNQ)$_2$ (**1**) and (MeO_2-bifc)(F_1-TCNQ)$_2$ (**2**) are monovalent 1:2 D/A salts, which can be represented as $[D]^+[A_2]^-$. These salts are comprised of valence-detrapped symmetric biferrocenium monocations, and exhibit mixed-stack and segregated-stack structures, respectively, despite their similar molecular shapes.

A packing diagram for **1** is shown in Figure 8a. The biferrocenium cations and acceptor dimers are located on inversion centers, forming a deformed CsCl-type crystal structure. The acceptor dimer is surrounded by eight cations and vice versa, in addition to the inter-dimer π–π contacts between the acceptor dimers, as seen in Figure 8b. This salt is isomorphous with the mixed-stack 1:2 D/A salts (R_2-bifc)(X_n-TCNQ)$_2$, where R = Et, SMe, SeMe, I; X = F, Cl; n = 1, 2.[13] It is reasonable for **1** to have a monovalent state similar to that of (MeS_2-bifc)(F_1-TCNQ)$_2$,[13] because the redox potentials and molecular volumes of Et_2- and MeS_2-bifc are approximately the same. The corresponding F_2-TCNQ salt, (Et_2-bifc)(F_2-TCNQ)$_2$, is divalent because of the stronger electron accepting ability of F_2-TCNQ.[13] These results exemplify valence control in the salts by using different F_n-TCNQ.

A packing diagram for **2** is shown in Figure 9. This salt has a segregated-stack structure isomorphous to (Br_2-bifc)(F_n-TCNQ)$_2$ [n = 1, 2].[15] Thus, the assembled structures of **1** and **2** are different despite their similar molecular shapes. It is also noteworthy that **2** has a monovalent state, despite the stronger electron donating ability and smaller molecular volume of its donor as compared to Et_2-bifc. The cyclic voltammogram of MeO_2-bifc in acetonitrile exhibited reversible half-wave redox potentials at $E_{1/2}^1$ = −0.21 V and $E_{1/2}^2$ = 0.11 V (vs. $[FeCp_2]^{+/0}$). These values are

lower by 0.06 V than those for Et_2-bifc ($E_{1/2}^1$ = −0.16 and $E_{1/2}^2$ = 0.18 V[13]). This salt was tentatively plotted on the monovalent-divalent phase diagram for mixed-stack salts as shown in Figure 3 (**2**, shown in parenthesis). As this salt is located on the lower-left side in the diagram, it can be predicted that **2** would have a divalent state if it had a mixed-stack structure. However, **2** was a monovalent solid, which led to the conclusion that the segregated-stack structure of this salt had a small Madelung energy.

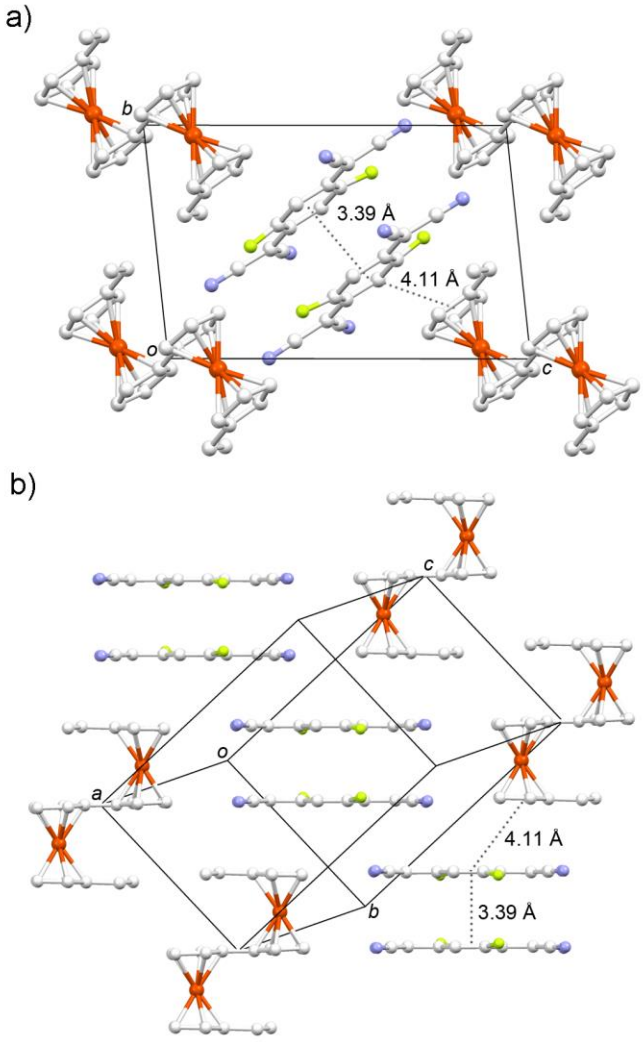

Figure 8. Packing diagram of (Et_2-bifc)(F_1-TCNQ)$_2$ (**1**) viewed (a) along the *a*-axis and (b) perpendicular to the stacking direction. Several intermolecular centroid–centroid distances are shown.

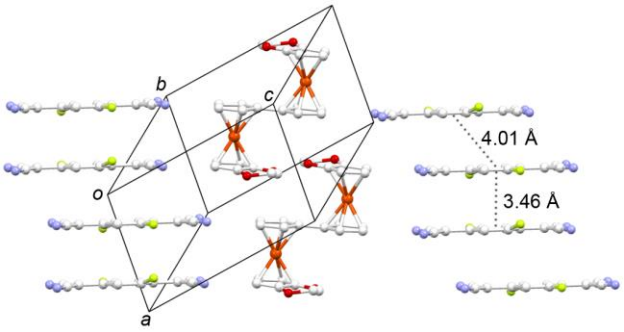

Figure 9. Packing diagram of $(MeO_2\text{-bifc})(F_1\text{-TCNQ})_2$ (**2**). Several intermolecular centroid–centroid distances are shown.

Structure of the intermediate-valence 2,6-F_2-TCNQ salt (3). $(MeS_2\text{-bifc})(2,6\text{-}F_2\text{-TCNQ})_2$ (**3**) is a 1:2 D/A salt with a mixed-stack structure and the unusual formal valence state of $[D]^{1.5+}[A_2]^{1.5-}$. A packing diagram for **3** at 100 K is shown in Figure 10. Its structure closely resembles that of **1**, as can be seen in Figure 8b. However, the unit cell volume in **3** is twice that of **1**, where the donor and acceptor dimer each have no inversion center. The dimer consists of crystallographically independent acceptors A1 and A2. It is intriguing that the orientation of the fluorine substituents in the dimer are the same, and the polar dimers are further arranged in a polar one-dimensional chain via interactions between the dicyanomethylene moieties (Figure 10). However, the dipole moments of the chains cancel out in the crystal because of the centrosymmetric space group.

The donor structure was observed as an averaged structure of $[D]^{2+}$ and $[D]^{+}$, which are disordered in a 1:1 ratio. The positive charge in the $[D]^{+}$ component is localized on the Fe1-containing ferrocenyl moiety, producing an unsymmetrical cation structure. Such valence trapping is often caused by electrostatic interactions with the acceptor.[11,14] It can be seen that Fe1 in **3** is surrounded by two electronegative cyano groups and two fluorine groups of the acceptors (Fe1⋯N = 4.32, 4.44 Å, Fe⋯F = 3.91, 3.80 Å). On the other hand, Fe2 is surrounded by two

cyano groups (Fe2···N = 4.33, 4.47 Å) and the ring hydrogens. Therefore, the charge localization on Fe1 is consistent with its stronger electrostatic interaction with the acceptors. Similarly, the larger negative charge for A2 (−0.80) than A1 (−0.67) in the acceptor dimer could probably be attributed to its stronger electrostatic interactions with cations; A2 is surrounded by seven cations and four F_1-TCNQ molecules, whereas A1 is surrounded by five cations and six F_1-TCNQ molecules.

This salt, containing 2,6-F_2-TCNQ, exhibits an intermediate valence state between the valence states of F_1-TCNQ salt (**3-F$_1$**, monovalent salt) and F_2-TCNQ salt (**3-F$_2$**, divalent salt), as also evident from the magnetic susceptibility data. **3-F$_1$** and **3-F$_2$** are both isomorphous to **1**, having a higher crystal symmetry than **3**. These salts were plotted on the monovalent-divalent phase diagram shown in Figure 3, where *V* for **3** was taken as half of its unit cell volume. Salt **3** had a larger *V* compared to **3-F$_2$** because of its intermediate valence state. It is noteworthy that 2,6-F_2-TCNQ and F_2-TCNQ produced salts with different valence states, despite their comparable electron accepting properties. The intermediate valence state in **3** could be attributed to the unsymmetrical crystalline environment around each molecule. The unsymmetrical charge distribution for $[D]^+$ and $[A_2]^-$ led to a shortening of the effective distance between the opposite charges, thereby increasing the Madelung energy of the monovalent state in **3** with respect to its divalent state. In addition, removing an electron from $[D]^+$ in **3** was less favorable because the neutral ferrocenyl moiety had lesser interactions with the anion compared with a salt with higher crystal symmetry. The same argument also applies to the acceptor. These factors, which make the divalent state less favorable, probably resulted in the intermediate valence state of **3**. Crystal structure determinations at 293−100 K and SQUID measurements (*vide ante*) showed that the valence state is temperature independent. X-ray diffraction patterns displayed no reflections corresponding to either a superstructure or phase separation. These results indicate that the

intermediate state is not the result of a transition between monovalent and divalent phases, but is instead a single phase in which $[D]^{+}$ and $[D]^{2+}$ form a static disorder. The static valence disorder in the as-grown crystal might be responsible for the temperature-independent valence state.

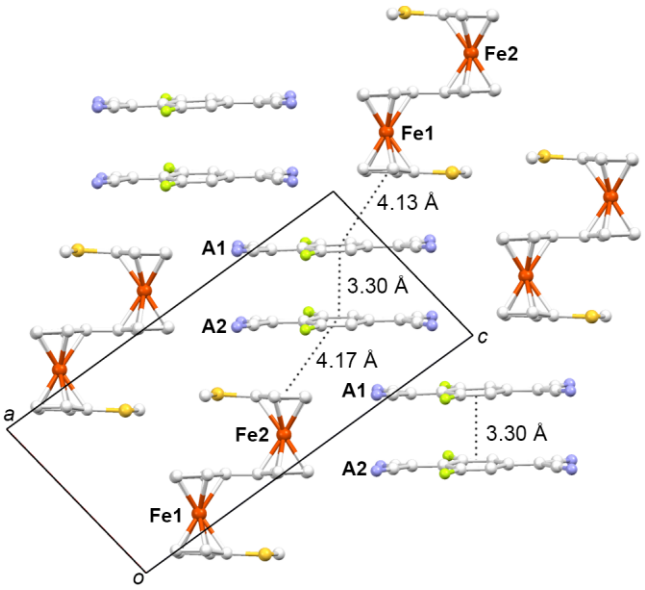

Figure 10. Packing diagram of (MeS_2-bifc)(2,6-F_2-TCNQ)$_2$ (**3**) at 100 K. Several intermolecular centroid–centroid distances are shown.

Structure of divalent F_1-TCNQ salt (4). (Bu_2-bifc)(F_1-TCNQ)$_3$ (**4**) is a divalent 1:3 D/A salt ($[D]^{2+}[A_3]^{2-}$) with a segregated-stack structure. The packing diagram of **4** is shown in Figure 11. This salt is isomorphous with the corresponding TCNQ salt (Bu_2-bifc)(TCNQ)$_3$,[19] which is a monovalent salt ($[D]^{+}[A_3]^{-}$). Thus, the introduction of a fluorine atom into the acceptor was also effective for the valence control of segregated-stack structures.

This salt contains a centrosymmetric dication. The acceptors produce one-dimensional columnar stacking, in which the crystallographically independent molecules (A1 and A2) are arranged as –A1–A1–A2–. A2 is located on the inversion center and exhibits a 1:1 disorder of the fluorine positions. The intermolecular centroid-centroid distances are 3.80 Å (A1–A1) and 3.78 Å

(A1–A2), indicating that the anion column is nearly uniform. The π–π interplanar distance for A1–A1 (3.19 Å) is shorter than that for A1–A2 (3.26 Å). This is consistent with the larger charge distribution on A1 than A2 (as estimated from the bond lengths, Table 1) filling the bonding orbital. The corresponding TCNQ salt, (Bu_2-bifc)$(TCNQ)_3$, is monovalent and has almost the same crystal structure as **4**. In this salt, the intermolecular centroid-centroid distances in the acceptor column are 3.86 Å (A1–A1) and 3.90 Å (A1–A2).[12] Therefore, the corresponding distances in **4** were shorter, which can be explained by the stronger bonding interactions between the acceptors having a larger negative charge density.

(Neopentyl$_2$-bifc)$(F_1$-TCNQ$)_3$ is known to undergo a phase transition from the monovalent to the divalent state at low temperatures.[10] Compared to this salt, the Madelung constant of **4** was expected to be smaller because of its segregated-stack structure. However, the smaller molecular volume for Bu_2-bifc in comparison with neopentyl$_2$-bifc increased its Madelung energy gain, which resulted in the divalent state of **4**. Indeed, the unit cell volume of **4** (1283 Å^3 at 100 K) is much smaller than that of (neopentyl$_2$-bifc)$(F_1$-TCNQ$)_3$ (1355 Å^3 at 90 K[10]) in the divalent phase. It is worth noting that the monovalent-divalent phase control by fluorine substitution is observed between **4** and (Bu_2-bifc)$(TCNQ)_3$ as well, which have segregated-stack structures. This stands in contrast to the case of organic charge-transfer complexes, for which neutral-ionic phase classification is specific to mixed-stack structures.[2] This phenomenon is mainly attributed to the small intermolecular transfer integrals in biferrocenium salts. Although **4** did not exhibit phase transition to a monovalent state even at a low temperature, it is highly probable that the molecular alloy of **4** and the monovalent TCNQ salt exhibit a valence transition, considering the phase behavior of (neopentyl$_2$-bifc)$(F_1$-TCNQ$)_{3-x}(TCNQ)_x$.[10a]

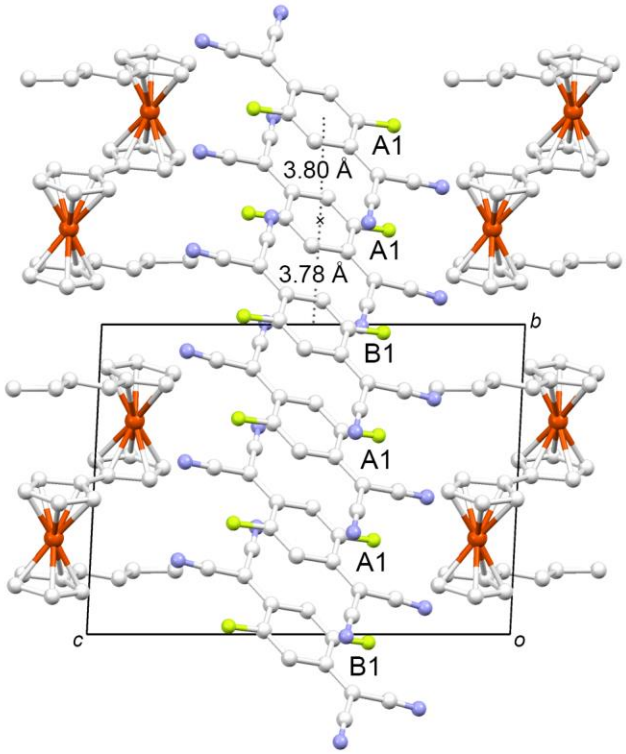

Figure 11. Packing diagram of (Bu_2-bifc)(F_1-TCNQ)$_3$ (**4**). Several intermolecular centroid–centroid distances are shown.

Structures of monovalent F_4-TCNQ salts (5 and 6). (R_2-bifc)(F_4-TCNQ) (**5**: R = Bu and **6**: R = I) are 1:1 D/A monovalent salts that can be represented as $[D]^+[A]^-$. These salts contain valence-trapped unsymmetrical cations and the acceptor is a monoanion that forms a diamagnetic dimer. The stoichiometry and valence states of these salts are similar to those of other F_4-TCNQ salts.[12,14] This feature is a result of the strong tendency of F_4-TCNQ to produce a monoanion and form a diamagnetic dimer, although there are examples of F_4-TCNQ salts with a different valence state.[14]

A packing diagram for **5** is shown in Figure 12a. In the cation, the butyl substituent on the Fe1-containing moiety is twisted and bent away from the Cp ring, whereas the other substituent exhibits an all-*trans* conformation. The Cp ring of the Fe1-containing moiety interacts with the

butyl group of the adjacent cation, whereas the Cp ring in the other moiety has π–π interactions with the acceptor molecule. The acceptor dimers have no mutual π–π contacts. When viewed perpendicular to the acceptor plane, the structure is regarded as a –D–D–A–A– type mixed-stack arrangement. The packing structure resembles that of (^{i}Bu$_2$-bifc)(F$_4$-TCNQ),[14] although the donor-acceptor arrangement is slightly different.

A packing diagram for **6**, which is a dichloromethane solvate, is shown in Figure 12b. The dichloromethane molecule, exhibiting a two-fold disorder, is located in a cavity surrounded by four cations and two acceptor molecules. In contrast to **5**, there are short contacts between the acceptor dimers at the dicyanomethylene moieties, which form a partially overlapped one-dimensional arrangement. The acceptor dimer has a π–π contact with a Cp ring in the cation. It is to be noted that the local D–D, A–A, and D–A arrangements resemble those in **1** and in the other 1:2 mixed-stack salts,[13] despite the different D/A ratios and valence states.

The valence localization of the cations in these salts is attributed to local Fe···NC– electrostatic interactions. The ferrocenyl moieties containing Fe1 and Fe2 are cationic and neutral, respectively, in both salts. In **5**, Fe1 is surrounded by four electronegative cyano groups (Fe···N distances are 4.34 Å and 4.36 Å), whereas only two cyano groups are close to Fe2 (Fe···N = 4.39 Å). Similarly, in salt **6**, the two cyano groups of the acceptors are close to Fe1 (Fe···N = 4.16, 4.29 Å), whereas only one cyano group is close to Fe2 (Fe···N = 4.28 Å). Therefore, in both salts, Fe1 more strongly interacts with the cyano groups than Fe2, which accounts for the valence trapping. Similar to these salts, other 1:1 D/A salts with F$_4$-TCNQ (or F$_2$-TCNQ) adopt the valence-trapped state based on their local electrostatic interactions.[14]

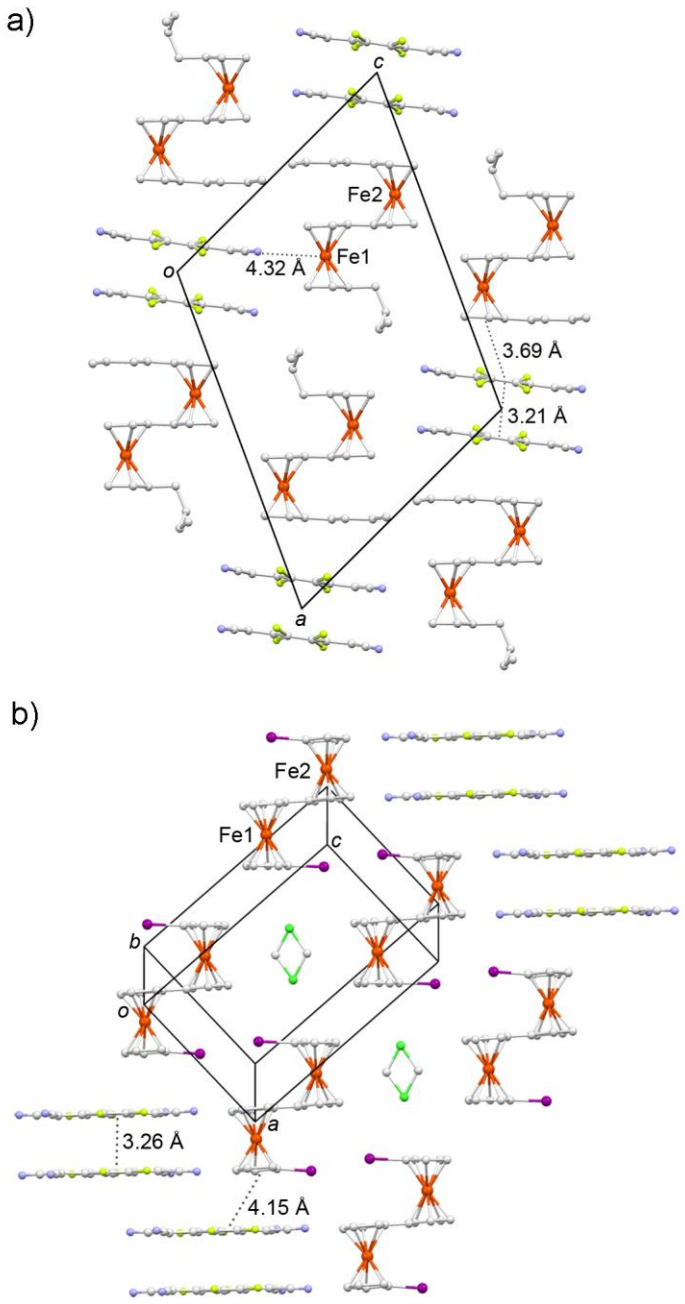

Figure 12. Packing diagrams of (a) (Bu_2-bifc)(F_4-TCNQ) (**5**) and (b) (I_2-bifc)(F_4-TCNQ)·0.5CH_2Cl_2 (**6**). The Fe1···NC– interaction in **5**, which results in a charge localization on Fe1, is drawn with dotted lines. Several intermolecular distances are also shown.

Redox potentials and crystal structure of CN_2-bifc. CN_2-bifc has low electron donating

ability because of the strong electron-withdrawing effect of the cyano group. The cyclic voltammogram of the CN_2-bifc measured in dichloromethane exhibited reversible redox waves at $E_{1/2}^1$ = 0.31 V (vs. $[FeCp_2]^{+/0}$) and an irreversible oxidation wave at E_{pa}^2 = 0.64 V. These values are much higher than those for biferrocene ($E_{1/2}^1$ = −0.09 V, $E_{1/2}^2$ = 0.23 V). This feature is probably responsible for its inability to form a salt with F_n-TCNQ. However, preliminary investigations revealed that 1′-cyano-biferrocene (CN_1-bifc) forms segregated-stack 1:2 D/A mixed-valent salts with F_2- and 2,3-Cl_2-TCNQ.[19]

A packing diagram for CN_2-bifc is shown in Figure 13. Each molecule is located on an inversion center. The Fe–Cp distance is 1.65 Å, which is reasonable for a neutral biferrocene. Hydrogen-bond-like intermolecular contacts could be observed between the cyano group and a CH hydrogen, with the –N···H– distance as 2.60 Å. This distance is shorter than the van der Waals distances by 0.15 Å.

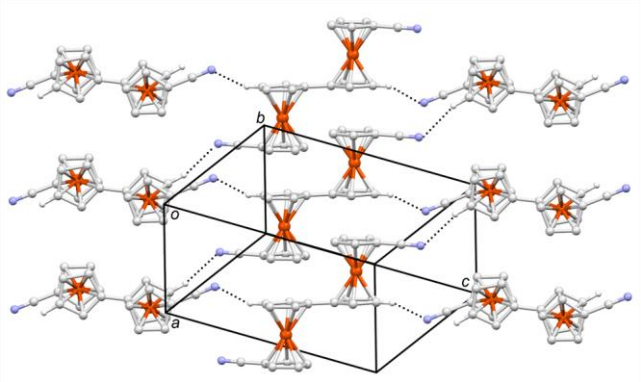

Figure 13. Packing diagram for CN_2-bifc. The dotted lines indicate hydrogen-bond-like intermolecular –N···HC– contacts.

CONCLUSION

In this work, the structural and magnetic properties of various biferrocenium salts with F_n-TCNQ were investigated. Most of the salts exhibited either the monovalent ($[D]^+[A_m]^-$) or the divalent

($[D]^+[A_m]^-$) state, depending on the balance between the redox potentials of the constituent molecules and their Madelung energies. Comparisons between (Et_2-bifc)(F_n-TCNQ)$_2$ (n = 1, 2) and (Bu_2-bifc)(F_n-TCNQ)$_3$ (n = 1, 0) demonstrated that valence control could be achieved by fluorine substitution of the acceptors, without changing the crystal structures. Valence control was also found to be possible for salts with segregated-stack structures. Furthermore, an intermediate valence state was found in (MeS_2-bifc)(2,6-F_2-TCNQ)$_2$, which is a single phase with a static disorder of $[D]^+$ and $[D]^{2+}$. This valence state likely exists as a result of the unsymmetrical crystal environment due to the polarity of the acceptor, which causes a smaller Madelung energy gain. The effect of the crystal structure on the Madelung energy was also evident in the segregated-stack salt (MeO_2-bifc)(F_1-TCNQ)$_2$, which has a monovalent state despite the low redox potential of the donor. On the other hand, F_4-TCNQ produced monovalent 1:1 D/A salts, similar to the case of other biferrocenes. Dicyano-biferrocene did not produce any salts with F_n-TCNQ because of its high redox potential.

This paper is the final part of our investigation into biferrocenium salts with organic acceptors, which began nearly 20 years ago.[20] Controlling valence states in ionic materials is an important objective for solid state electronics. With this study and our previous research, we have elucidated the correlation between the structures, redox potentials, and valence states of biferrocenium salts, and illustrated the means for enabling valency control of ionic crystals, i.e., via molecular modification and crystal engineering approaches. The concepts outlined in these studies can be extended to other molecular materials as well.

EXPERIMENTAL

General. 1′,1‴-R_2-1,1″-biferrocene (R = I,[21] Bu,[22] MeS,[23] Et,[24]), F_1-TCNQ,[25] and 2,6-F_2-TCNQ[25] were synthesized according to methods reported in the literature. F_4-TCNQ was

purchased from TCI. ^{1}H NMR spectra were recorded on a JOEL JNM-ECL-400 spectrometer. Mass spectra were obtained by positive ion electrospray using LTQ Orbitrap Discovery (Thermo Fisher Scientific). Infrared spectra were recorded on a Thermo Scientific Nicolet iS5 FT-IR spectrometer via attenuated total reflectance (ATR, diamond). Magnetic susceptibilities were measured using a Quantum Design MPMS-XL instrument under 0.5 T. The low S/N ratio in the susceptibility data of **4** is due to the small sample mass (1.4 mg). Cyclic voltammograms of MeO_2-bifc and CN_2-bifc were recorded with an ALS/chi electrochemical analyzer model 600A. Redox potentials were measured at a scan rate of 0.1 V s^{-1} in a 0.1 mM solution of the compound in acetonitrile containing 0.1 mol dm^{-3} *n*-Bu_4NClO_4 as the supporting electrolyte. The Ag/Ag^+ and Pt wire electrodes were used as the reference and working electrodes, respectively.

Synthesis of 1′,1‴-dimethoxy-1,1″-biferrocene (MeO_2-bifc). (a) 1′,1‴-Diacetoxy-1,1″-biferrocene. Under a nitrogen atmosphere, a mixture of 1′,1‴-dibromobiferrocene (1.00 g, 1.89 mmol), Cu_2O (0.541 g, 3.78 mmol), acetic acid (0.22 mL, 3.78 mmol), and acetonitrile (20 mL) was heated at 95 °C for 15 h with continuous stirring. After cooling to room temperature, the reaction mixture was filtered through celite and the filtrate was evaporated under reduced pressure. The residue was purified by column chromatography (silica gel, eluent: toluene). The first, second, and third bands produced biferrocene (60 mg), acetoxybiferrocene (35 mg), and 1′,1‴-diacetoxy-1,1″-biferrocene (120 mg, yield 13%), respectively. ^{1}H NMR ($CDCl_3$, TMS): δ 2.00 (s, 6H), 3.78 (t, 4H, J = 1.9 Hz), 4.23 (t, 4H, J = 1.9 Hz), 4.28 (t, 4H, J = 1.9 Hz), 4.41 (t, 4H, J = 1.9 Hz). **(b) 1′,1‴-Dimethoxy-1,1″-biferrocene.** Under a nitrogen atmosphere, NaH (0.148 g, 2.47 mmol) was added to a solution of 1′,1‴-diacetoxy-1,1″-biferrocene (120 mg, 0.247 mmol), 15-crown-5 (0.032 mL, 0.16 mmol), and CH_3I (0.11 mL, 1.7 mmol) in THF (15 mL). After stirring for 15 h, the reaction mixture was filtered through celite and the solvent was evaporated under reduced pressure. The residue was

passed through a short column of silica gel (eluent: toluene). The evaporation of the solution produced the desired product as brown needle-like crystals (85 mg, 80%), which were further recrystallized from hexane (55 mg, 51%). ^{1}H NMR ($CDCl_3$, TMS): δ 3.47 (s, 6H), 3.67 (t, 4H, *J* = 1.8 Hz), 3.88 (t, 4H, *J* = 1.8 Hz), 4.21 (t, 4H, *J* = 1.8 Hz), 4.40 (t, 4H, *J* = 1.8 Hz). HRMS-ESI (*m*/*z*): $[M]^+$ calcd for $C_{22}H_{22}Fe_2O_2$, 430.0319; found, 430.0325.

Synthesis of 1′,1‴-dicyano-1,1″-biferrocene (CN_2-bifc). This compound was prepared following the literature method,[21] although the product was not isolated in the previous report. A mixture of I_2-bifc (1.46 g, 2.35 mmol) and CuCN (4.20 g, 46.9 mmol) was heated under a nitrogen atmosphere at 180 °C for 2 h. The reaction mixture was repeatedly extracted with dichloromethane and purified by column chromatography (alumina, eluent: hexane–dichloromethane). The desired product was obtained as a dark yellow powder (0.18 g, yield 18%), which was further recrystallized from dichloromethane–hexane (1:1, *v*/*v*). ^{1}H NMR ($CDCl_3$, TMS): δ = 4.23 (t, 4H, *J* = 2.0 Hz), 4.43 (m, 8H), 4.56 (t, 4H, *J* = 1.8 Hz). IR (cm^{-1}): ν = 554, 811, 827, 841, 2223 (CN). HRMS-ESI (*m*/*z*): $[M+H]^+$ calcd for $C_{22}H_{17}N_2Fe_2$, 421.0091; found, 421.0090. Single crystals of CN_2-bifc were grown by the slow evaporation of its dichloromethane solution.

Preparation of salts. Single crystals of **2** were prepared as follows. The solutions of MeO_2-Bifc (10.0 mg, 23×10^{-3} mmol) in 1,2-dichloroethane (2.5 mL) and F_1-TCNQ (9.2 mg, 41×10^{-3} mmol) in 1,2-dichloroethane (2.5 mL) were mixed and filtered. The vapor diffusion of pentane into this solution produced fine needle-like brown crystals of **2** (12.2 mg, yield 61%). Anal. Calcd for $C_{46}H_{28}F_2Fe_2N_8O_2$: C, 63.18; H, 3.23; N, 12.81. Found C, 63.20; H, 3.30; N, 12.60. IR (cm^{-1}): 2172, 2198 (CN). Single crystals of **1**, **3**, and **4** were obtained similarly, except that **4** was obtained in a low yield by the vapor diffusion of pentane into a chloroform solution of the

components. **1**: HRMS-ESI (*m*/*z*): $[M]^+$ calcd for $C_{24}H_{26}Fe_2$, 426.0733; found, 426.0733; $[M]^-$ calcd for $C_{12}H_3FN_4$, 222.0342; found, 222.0355. IR (cm^{-1}): 2178 (CN). **3**: HRMS-ESI (*m*/*z*): $[M]^+$ calcd for $C_{22}H_{22}Fe_2S_2$, 461.9862; found, 461.9874; $[M]^-$ calcd for $C_{12}H_2F_2N_4$, 240.0248; found, 240.0255. IR (cm^{-1}): 2150, 2176 (CN). **4**: Anal. Calcd for $C_{64}H_{43}F_3Fe_2N_{12}$: C, 66.91; H, 3.77; N, 14.63. Found C, 66.68; H, 3.77; N, 14.31. Salt **5** was prepared as follows. I_2-bifc (5 mg, 8.0×10^{-3} mmol) and F_4-TCNQ (2.2 mg, 8.0×10^{-3} mmol) were dissolved in a mixture of dichloromethane and a small amount of acetone (4 mL) with heating. The solution was concentrated to approximately 0.5 mL, and then slowly cooled to produce black crystals of **5**, which were collected and dried under vacuum (5.5 mg, 76% yield). Anal. Calcd for $C_{32}H_{16}N_4F_4Fe_2I_2$: C, 42.80; H, 1.80; N, 6.24. Found: C, 42.62; H, 2.19; N, 5.93. IR (cm^{-1}): 2197, 2192, 2178 (CN). **6** was prepared by the same method using Bu_2-bifc (black block crystals, 41% yield). Anal. Calcd for $C_{40}H_{34}N_4F_4Fe_2$: C, 63.34; H, 4.52; N, 7.39. Found: C 63.35; H, 4.56; N, 7.39. IR (cm^{-1}): 2197, 2176 (CN).

X-ray crystallography. Single crystal X-ray diffraction data were collected using MoKα radiation on Bruker APEX II Ultra, Rigaku Mercury (for **5**), and Rigaku AFC-5S (for CN_2-bifc) diffractometers. All calculations were performed using SHELXTL[26] and the structures were solved by direct methods (SHELXS 97). The butyl substituents in **4** exhibited elongated thermal ellipsoids (indicative of disorder but not resolved). ORTEP-3 for Windows[27] and Mercury[28] was used to produce molecular graphics. Crystallographic parameters are listed in Tables 4 and 5.

Table 4. Crystallographic parameters.

	1	**2**	**3** (100 K)	**3** (200 K)	**3** (293 K)
Empirical formula	$C_{48}H_{32}F_2Fe_2N_8$	$C_{48}H_{32}F_2Fe_2N_8$	$C_{46}H_{26}F_4Fe_2N_8S_2$		
Formula weight	870.51	874.46	942.57		
Crystal system	Triclinic	triclinic	triclinic	triclinic	triclinic
Space group	*P*–1	*P*–1	*P*–1	*P*–1	*P*–1

a / Å	8.547(2)	7.094(3)	8.9542(13)	9.0093(9)	9.0708(10)
b / Å	9.064(3)	8.812(4)	12.0583(17)	12.1222(12)	12.1805(13)
c / Å	13.743(4)	16.467(7)	18.025(3)	18.0422(18)	18.0494(19)
α / deg	90.855(4)	95.401(6)	90.595(2)	90.4200(10)	90.338(2)
β / deg	104.816(4)	101.318(6)	98.122(2)	97.8930(10)	97.6420(10)
γ / deg	108.775(4)	112.269(6)	93.353(2)	92.9820(10)	92.519(2)
V / Å	969.0(5)	917.9(6)	1923.0(5)	1948.9(3)	1974.5(4)
Z value	1	1	2	2	2
ρ_{calcd} / g cm^{-3}	1.492	1.582	1.628	1.606	1.585
F (000)	446	446	956	956	956
Reflections collected	4661	5506	11022	10585	10706
Independent reflections	3466	3859	8215	7783	7883
Parameters	282	300	561	561	561
Temperature / K	100	173	100	200	293
R_1, R_w ($I > 2\sigma$) [a]	0.0429, 0.1086	0.0668, 0.1528	0.0540, 0.1522	0.0329, 0.0860	0.0415, 0.1050
R_1, R_w (all data) [a]	0.0489, 0.1116	0.1084, 0.1732	0.0584, 0.1571	0.0411, 0.0909	0.0584, 0.1153
Goodness of fit	1.068	1.029	1.021	1.043	1.03

[a] $R_1 = \Sigma||F_o| - |F_c|| / \Sigma|F_o|$, $R_w = [\Sigma w (F_o^2 - F_c^2)^2 / \Sigma w (F_o^2)^2]^{1/2}$.

Table 5. Crystallographic parameters.

	4	**5**	**6**	CN_2-bifc
Empirical formula	$C_{64}H_{43}F_3Fe_2N_{12}$	$C_{40}H_{34}F_4Fe_2N_4$	$C_{32.5}H_{17}Cl_1F_4Fe_2I_2N_4$	$C_{22}H_{16}Fe_2N_2$
Formula weight	1148.8	758.41	940.45	420.07
Crystal system	Triclinic	monoclinic	triclinic	monoclinic
Space group	P–1	$C2/m$	P–1	$P2_1/c$
a / Å	8.43(2)	19.89(3)	9.175(6)	8.948(2)
b / Å	11.36(3)	12.080(14)	12.396(8)	7.4218(18)
c / Å	14.62(3)	15.62(2)	13.632(9)	12.797(2)
a / deg	89.08(4)	90	89.187(11)	90
b / deg	80.46(3)	114.73(2)	89.885(11)	101.730(16)
g / deg	68.54(3)	90	87.936(11)	90
V / Å	1283(5)	3410(8)	1549.2(18)	832.1(3)
Z value	1	4	2	2
r_{calcd} / g cm^{-3}	1.487	1.477	2.016	1.677
F (000)	590	1560	902	428
Reflections collected	5402	11976	10094	1612
Independent reflections	5402	2398	5360	1512
Parameters	381	287	415	118
Temperature / K	100	100	293	296
R_1, R_w ($I > 2\sigma$) [a]	0.0952, 0.2382	0.0897, 0.2700	0.0749, 0.1950	0.0300, 0.0834
R_1, R_w (all data) [a]	0.1379, 0.2626	0.9570, 0.2758	0.0940, 0.2093	0.0458, 0.0893
Goodness of fit	1.001	0.924	1.042	1.169

[a] $R_1 = \Sigma||F_o| - |F_c|| / \Sigma|F_o|$, $R_w = [\Sigma w (F_o^2 - F_c^2)^2 / \Sigma w (F_o^2)^2]^{1/2}$.

ASSOCIATED CONTENT

Accession Codes

CCDC-1548116 (**1**), -1548151 (**2**), -1548117 (**3**, at 100 K), -1556793 (**3**, at 200 K), -1556794 (**3**, at 293 K), -1548097 (**4**), -1019740 (**5**), -1019739 (**6**), and -1038141 (CN_2-bifc) contain the supplementary crystallographic data for this paper. These data can be obtained free of charge from The Cambridge Crystallographic Data Centre via www.ccdc.cam.ac.uk/data_request/cif.

AUTHOR INFORMATION

Corresponding Author

*E-mail: tmochida@platinum.kobe-u.ac.jp. Tel/Fax: +81-78-803-5679.

ORCID

Tomoyuki Mochida: 0000-0002-3446-2145

Yusuke Funasako: 0000-0002-1523-9730

Notes

The authors declare no competing financial interest.

ACKNOWLEDGMENTS

This work was financially supported by KAKENHI (Grant No. 16H04132) from the Japan Society for the Promotion of Science (JSPS). We also thank Shizue Yamazaki and Takahiro Akasaka (Toho University) for their help with sample preparation.

REFERENCES

(1) (a) Ouahab, L.; Yagubskii, E. *Organic Conductors, Superconductors and Magnets: From*

Synthesis to Molecular Electronics, ed., Springer **2004**. (b) Fourmigué, M.; Ouahab, L. *Conducting and magnetic Organometallic Molecular Materials*, Topics in Organometallic Chemistry, ed. Springer, vol. 27, **2009**. (c) Saito G.; Yoshida Y. *Bull. Chem. Soc. Jpn.*, **2007**, 80, 1–137.

(2) (a) Torrance, J. B.; Vazquez, J. E.; Mayerle, J. J.; Lee, V. Y. *Phys. Rev. Lett*. **1981**, 46, 253–257. (b) Horiuchi, S.; Okimoto, Y.; Kumai, R.; Tokura, Y. *Science* **2003**, 299, 299. (c) Collet, E.; Lemée-Cailleau, M.-H.; Cointe, M. B.-L.; Cailleau, H.; Wulff, M.; Luty, T.; Koshihara, S.; Meyer, M.; Toupet, L.; Rabiller, P.; Techert, S. *Science* **2003**, 300, 612–615.

(3) Hendrickson, D. N. In *Mixed Valency Systems: Applications in Chemistry, Physics, and Biology, Series* Prassides, *C.* K. (Ed.), NATO ASI Series, Vol. 343, pp. 67−90, Kluwer, Dordrecht **1991**.

(4) Morrison, W. H.; Hendrickson, D. N. *Inorg. Chem.* **1975**, 14, 2331–2346.

(5) Dong, T.-Y.; Chang, L.-S.; Lee, G.-H.; Peng, S.-M. *Organometallics* **2002**, 21, 4192−4200.

(6) Sano, H. *Hyperfine Interact.* **1990**, 53, 97−112.

(7) Nakashima, S.; Masuda, Y.; Motoyama, I.; Sano, H. *Bull. Chem. Soc. Jpn*. **1987**, 60, 1673–1680.

(8) Iijima, S.; Mizutani, F. *Mol. Cryst. Liq. Cryst*. **1998**, 322, 79.

(9) Nakashima, S.; Iijima, S.; Motoyama, I.; Katada, M.; Sano, H. *Hyperfine Interact*. **1988**, 40, 315.

(10) (a) Mochida, T.; Funasako, Y.; Takazawa, K.; Takahashi, M.; Matsushita, M. M.; Sugawara, T. *Chem. Commun*. **2014**, 50, 5473–5475. (b) Mochida, T.; Takazawa, K.; Takahashi, M.; Takeda, M.; Nishio, Y.; Sato, M.; Kajita, K.; Mori, H.; Matsushita, M. M.; Sugawara, T. *J. Phys. Soc. Jpn*. **2005**, 74, 2214−2216. (c) Uruichi, M.; Yue, Y.; Yakushi, K.; Mochida, T. *J. Phys. Soc. Jpn.* **2007**, 76, 124707/1–6.

(11) Mochida, T.; Takazawa, K.; Matsui, H.; Takahashi, M.; Takeda, M.; Sato, M.; Nishio, Y.; Kajita, K.; Mori, H. *Inorg. Chem*. **2005**, 44, 8628−8641.

(12) Mochida, T.; Yamazaki, S.; Suzuki, S.; Shimizu, S.; Mori, H. *Bull. Chem. Soc. Jpn.* **2003**, 76, 2321–2328.

(13) Mochida, T.; Funasako, Y.; Akasaka, T.; Uruichi, M.; Mori, H. *CrystEngComm* **2017**, 19, 1449–1453.

(14) Mochida, T.; Funasako, Y.; Nagabuchi, E.; Mori, H. *Cryst. Growth Des*. **2014**, 14,

1459–1466.

(15) Mochida, T.; Funasako, Y.; Yamazaki, S.; Mori, H. *Eur. J. Inorg. Chem.* **2014**, 24, 3920–3926.

(16) (a) Mochida, T.; Nagabuchi, E.; Takahashi, M.; Mori, H. *Chem. Commun*. **2014**, 50, 2481–2483. (b) Mochida, T.; Funasako, Y.; Takahashi, K.; Inokuchi, M.; Sakurai, T.; Ikeda, S.; Ohta, H.; Mori, H.; Uruichi, M. *Chem. Commun.* **2014**, 50, 13370–13372.

(17) (a) Funasako, Y.; Mochida, T.; Sakurai, T.; Ohta, H.; Akasaka, T.; Nishio, Y. *Inorg. Chim. Acta* **2014**, 419, 105–110. (b) Mochida, T.; Moriyama, H.; Hasegawa, T.; Kondo, R.; Kagoshima, S.; Iwasa, Y. *Synth. Met*. **1999**, 86, 1678.

(18) Kistenmacher, T. J.; Emage, T. J.; Bloch, A. N.; Cowan, D. O. *Acta Crystallogr*. **1982**, B38, 1193−1199.

(19) Kato, K.; Mochida, T. unpublished results.

(20) Mochida, T. *Mol. Cryst. Liq. Cryst*. **2000**, 343, 205–210.

(21) Kovar, R. F.; Rausch, M. D.; Rosenberg, H. *Organomet. Chem. Syn.* **1971**, 1, 173–181.

(22) Dong, T. -Y.; Hendrickson, D. N.; Iwai, K.; Cohn, M. J.; Geib, S. J.; Rheingold, A. L.; Sano, H.; Motoyama, I.; Nakashima, S. *J. Am. Chem. Soc*. **1985**, 107, 7996.

(23) Dong, T. -Y.; Chang, C. -K.; Lee, S. -H.; Lai, L. -L.; Chiang, M. Y. -N.; Lin, K. -J. *Organometallics* **1997**, 16, 5816–5825.

(24) Iijima, S.; Sada, R.; Motoyama, I.; Sano, H. *Bull. Chem. Soc. Jpn.* **1981**, 54, 1375–1379.

(25) Mochida, T.; Hasegawa, T.; Kagoshima, S.; Sugiura, S.; Iwasa, Y. *Synth. Met*. **1997**, 86, 1797–1798.

(26) Sheldrick, G. M. *Acta Crystallogr*. **2008**, A64, 112–122.

(27) Farrugia, L. J. *J. Appl. Crystallogr*. **1999**, *32*, 837–838.

(28) Macrae, C. F.; Bruno, I. J.; Chisholm, J. A.; Edgington, P. R.; McCabe, P.; Pidcock, E.; Rodriguez-Monge, L.; Taylor, R.; van de Streek, J.; Wood, P. A. *J. Appl. Crystallogr*. **2008**, *41*, 466−470.

Table of Contents Use Only

SYNOPSIS. The crystal structures and valence states of salts composed of 1′,1‴-disubstituted biferrocene derivatives (D) and F_n-TCNQ (A; n = 1, 2, 4) have been investigated. These salts exhibited either monovalent ($[D]^{+}[A_m]^{-}$; m = 1–3), divalent ($[D]^{2+}[A_m]^{2-}$), or intermediate valence states, which could be controlled by changing the substituents.